Fabrication and characterization of Nano (H$_2$dabco)[K(ClO$_4$)$_3$] molecular Perovskite by ball milling

Qi Jia, Xueyuan Bai, Shaoyong Zhu, Xiong Cao, Peng Deng & Lishuang Hu

Published online: 13 Dec 2019.

Submit your article to this journal ☑

View related articles ☑

View Crossmark data ☑

Taylor & Francis
Taylor & Francis Group

Check for updates

Fabrication and characterization of Nano (H$_2$dabco)[K(ClO$_4$)$_3$] molecular Perovskite by ball milling

Qi Jia[a], Xueyuan Bai[b], Shaoyong Zhu[c], Xiong Cao[a], Peng Deng[d], and Lishuang Hu[a]

[a]School of Environment and Safety Engineering, North University of China, Taiyuan, China; [b]Sichuan Police college, Luzhou, Sichuan Province, P.R.China; [c]Gas Center of Siming, Xiamen, Fujian Province, P.R.China; [d]State Key Laboratory of Explosion Science and Technology, Beijing Institute of Technology, Beijing, PR China

ABSTRACT

Nano (H$_2$dabco)[K(ClO$_4$)$_3$] (DAP-2) were successfully prepared via the milling method. The morphology and structure of the as-obtained sample were characterized by scanning electron microscopy (SEM), X-ray diffraction (XRD) and Fourier transform infrared spectroscopy (FT-IR). The results showed the nano DAP-2 with nearly spherical morphologies have a narrow particle size distribution ranged from 1μm to 2μm. The thermal decomposition properties were investigated by thermogravimetric-differential scanning calorimeter (TG-DSC). The exothermal peak of nano DAP-2 thermal decomposition is 384.5°C decreased by 6.7°C compared with raw DAP-2 (391.2°C). And the apparent activation energy (E_a) of nano DAP-2 was calculated as 173.346 kJ mol^{-1} by Kissinger equation, which is lower than raw DAP-2 (177.699 kJ·mol^{-1}). Sensitivity study showed that the nano DAP-2 (H$_{50}$: 60.63 cm) exhibited lower impact sensitivity than raw DAP-2 (H$_{50}$: 36.79 cm). Therefore, this work provides a simple and effective way to improve the thermal decomposition properties and safety performance of molecular perovskite energetic materials.

Introduction

With the continuous upgrading of weapons, modern high-tech warfare puts higher demands on energetic materials, such as higher energy, better safety, better reliability and more environmentally friendly. Humans have made rapid progress in developing high-energetic materials, such as nitrogen-rich molecules (Hermann et al. 2017; Xu et al. 2017), energetic co-crystals (Bolton and Matzger 2011), energetic salts (Liu, W L, and Pang 2017; Tang et al. 2017), as well as metal-organic frameworks (Li et al. 2013; Wang et al. 2017; Zhang et al. 2016).

Molecular assembly strategy could control the arrangement of molecular components effectively based on the interaction of intermolecular non-covalent bonds (hydrogen bonds, van der Waals forces, electrostatic forces, etc.), which has attracted much attention in the design of high-performance and insensitivity energetic materials (Bennion et al. 2016; Liu et al. 2018; Wang et al. 2016, 2019; Xu et al. 2019). Recently, Chen et al. (2018a, 2018b) proposed a novel, pioneering idea for design and fabrication of molecular perovskite energetic materials, combined with inorganic oxidative ClO$_4^-$ anions and reductive H$_2$dabco$_2^+$ cations (1,4-diazabicyclo[2.2.2]octane-1,4-diium) into a ternary high-symmetry cell with a general formula of ABX$_3$ perovskite structure, and obtained four molecular perovskite high-energeticmaterials (H$_2$dabco)[M(ClO$_4$)$_3$] (M = Na$^+$, K$^+$, Rb$^+$, and NH$_4^+$ for DAP-1, −2, −3, and −4, respectively). As an important one of the molecular perovskite energetic materials (H$_2$dabco)[K(ClO$_4$)$_3$] (DAP-2, dabco = 1,4-diazabicyclo [2.2.2] octane) can be synthesized by the one-pot reaction of dabco, KClO$_4$, and HClO$_4$ in a molar ratio of 1:1:2 at room

temperature. This facile and green molecular assembly strategy was also considered to be a significant avenue for designing the novel high-energetic materials (theoretical evaluations detonation velocity, detonation pressure, and detonation heats: 8.591 km·s^{-1} and 35.2 GPa and 6.12 kJ·g^{-1}, respectively) and good thermostable property. However, the weak safety performance (impact sensitivity: 16 J; friction sensitivity: 42 N) seriously restricted the potential applications of the molecular perovskite DAP-2 in the field of weapons and ammunition. It is necessary to introduce appropriate measures to adjust and enhance its safety performance to meet their future requirements (Cao et al. 2018a; Deng et al. 2017; Deng et al. 2019b; Li et al. 2020).

Mechanical ball milling technology, as an effective top-to-down method in nanoscience and technology, have attracted much attention in the fields of magnetic properties, electronics, energy, chemical industry, environmental protection, biological medicine and so on (Mo et al. 2019a, 2019b; Chen et al. 2020; Hassanin et al. 2018; Lei et al. 2019; Tiruye et al. 2017; Zhang et al. 2018; Deng et al. 2020; Wang et al, 2019). Especially in energetic materials, the mechanical ball milling technology is regarded as an important green and environmentally friendly technique for explosive refinement, because of high technology output, less/no use of organic solvents, moderate reaction temperature, safe, simple and controllable preparation process, short cycle and non-toxicity from this method. Generally, the particle size of the explosive had been reduced to the micro/nanoscale, the nano-sized explosive will exhibit some differences from those of the micrometer (Cao et al. 2018b; Cao et al. 2019; Deng et al. 2018), such as better stability and safety, and faster energy release and so on (Guo et al. 2015; Qiu et al. 2015). For example, Qiu et al. (2015) reported reduced-insensitivity CL-20/HMX (2,4,6,8,10,12-hexanitro-2,4,6,8,10,12-hexaazaisowurtzitane/1,3,5,7-tetranitro-1,3,5,7-tetrazocine) co-crystal with mean size below 200 nm can be prepared by bead-milling method. And Guo et al. (2015) used a mechanical ball milling method to produce nano-sized CL-20 with the average particle size of 200 nm. The thermal decomposition peak temperature of the nano CL-20 significantly become lower than that of micro-sized CL-20. And the impact and friction sensitivity had reduced clearly by 116.2% and 22%, respectively. These results revealed that the safety performance of nano-sized energetic materials have been greatly improved by the ball milling nano-sized technology. Therefore, it is promising to introduce ball milling technology to reduce the sensitivity of DAP-2.

In this work, molecular perovskite DAP-2 energetic material was synthesized via the molecular assembly strategy by facile one-pot reaction of dabco, KClO$_4$, and HClO$_4$. Nano DAP-2 was prepared by mechanical ball milling technology. The thermal decomposition and impact sensitivity properties of as-obtained samples were investigated. The morphology, thermal decomposition characteristics and mechanical impact sensitivity of DAP-2 samples before and after ball milling were discussed. This work aims to provide a reference for practical applications of molecular perovskite energetic materials in the future.

Experimental

Materials

The potassium perchlorate (KClO$_4$) and perchloric acid (70%) were provided by Shanxi Jiangyang Chem. Eng. Co., Ltd. The 1,4-diazabicyclo [2.2.2] octane was provided by Shanghai Aladdin Biochemical Technology Co., Ltd. Deionized water was obtained by a Milli-Q apparatus (Millipore).

Sample Preparation

The (H$_2$dabco)[K(ClO$_4$)$_3$] (DAP-2) was synthesized by adding 0.163 ml H$_2$0 solution with 70% perchloric acid (2 mmol) to a mixed solution (20 mL) of triethylenediamine (1 mmol) and potassium perchlorate (1 mmol) at room temperature. Then, keep at room temperature after heating to dissolve completely. The colorless products were obtained after filtered, washed, and dried.

The nano DAP-2 particles were prepared by ball milling method. Briefly, 5 g DAP-2 was milled dispersed in absolute ethanol under stirring (500 rpm) for 6 h. After filtration and drying, the nano DAP-2 samples were obtained.

Characterization

Powder X-ray diffraction (XRD) patterns were recorded on a Philips X'Pert Pro X-ray diffractometer (PANalytical, Holland) by using Cu-Kα (40 kV, 30 mA) radiation with λ = 0.15418 nm. The diffracted X-rays were collected from 5° to 45° with a step size of 0.05. Scanning electron microscopy (SEM) images were collected by the Ultra 55 microscope (Zeiss, the German). Fourier transform infrared (FT-IR) spectra of the samples was recorded with a Thermo Scientific Nicolet iS10 spectrophotometer. Samples were measured in 4000–650 cm^{-1} wave number range with 1 cm^{-1} resolution. Thermal performances analysis were performed on a STA449F3 Jupiter thermos-gravimetric differential scanning calorimeter (TG-DSC, Netzsch, Germany) at heating rates (5, 10, 15, and 20° C·min^{-1}) over the temperature range of 40–500°C. The impact sensitivity was tested with type 12 drop hammer apparatus. In the environment of 20–25°C room temperature and 40–45% relative humidity, 25 drop tests were conducted to calculate H_{50} with a drop hammer of 2.5 ± 0.003 kg and the dose was 35 ± 1 mg.

Results and Discussion

The size and morphology of raw and nano DAP-2 were observed by SEM. As shown in Figure 1a, the raw DAP-2 had a cubic shape with an edge length of about 300 μm. As shown in Figure 1b, the DAP-2 prepared by ball milling technique had a lower size with a narrow distribution range of 1 μm to 2 μm. After ball milling, nano DAP-2 had ellipsoidal shape and the surface became uniform and smooth, eliminating the sharp edges of raw DAP-2. This is due to the continuous collision, extrusion, shearing, and impact of zirconia balls during ball milling, which makes the particle size of DAP-2 reduced significantly and the sharp edges disappeared. That indicated the near-elliptical nanostructure of DAP-2 has been successfully prepared.

The XRD patterns of raw and nano DAP-2 were showed in Figure 2. The nano DAP-2 exhibited almost same diffraction peaks as raw DAP-2 at 12.46°, 21.55°, 24.98°, 27.88°, 37.14°, 37.68°, which are assigned to the crystal planes (200), (222), (400), (420), (531), and (600) of molecular perovskite DAP-2 (CCDC: 1528106), respectively. That demonstrated as-obtained nano DAP-2 had maintained the stable crystal phase after the milling process. The intensities of diffraction peaks of as-prepared samples reduced obviously compared with raw DAP-2, resulted from the change of exposure probability of different
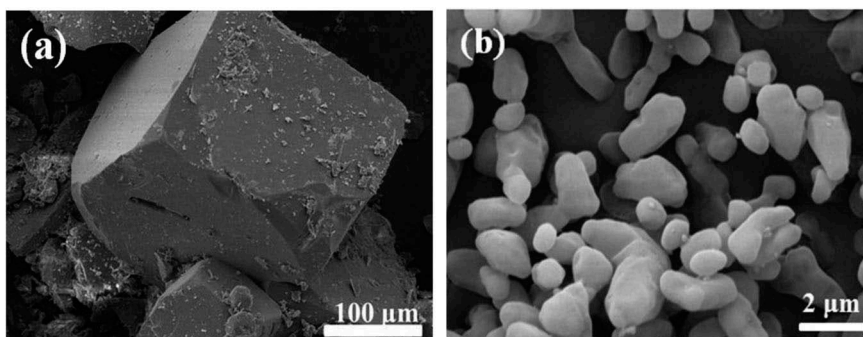

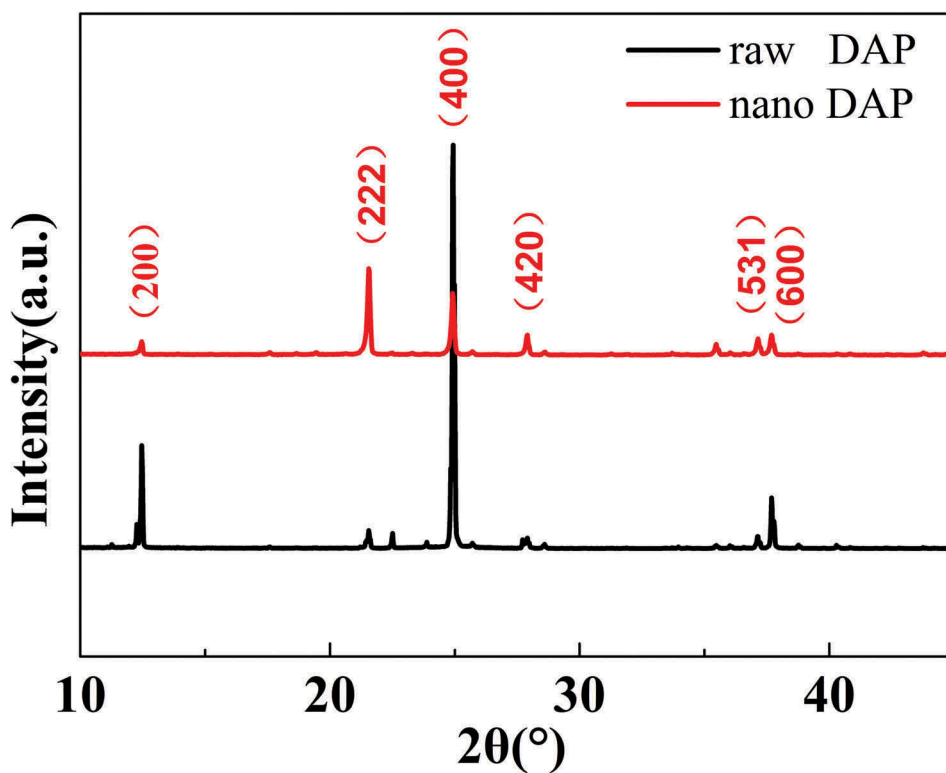Figure 1. SEM images of (a) raw and (b) nano DAP-2.

Figure 2. The XRD patterns of raw materials and milling DAP-2.

crystal planes for diffraction signal, which revealed the morphology of as-prepared samples have changed to some extent. That indicated the formation of nano-sized DAP-2 materials.

The FT-IR spectrum data were tabulated in Table 1. As to $KClO_4$, the IR peaks at 1061 and 939 cm^{-1} belongs to ClO_4^-. As to dabco, the spectrum peaks at 3235, 2937 cm^{-1} corresponds to C-H stretching and deformation vibrations, the spectrum peaks at 2870, 1678, 1455 cm^{-1} corresponds to CH_2 vibrations, the spectrum peaks at 1314 cm^{-1} corresponds to C-N stretching vibrations, the spectrum peaks at 1056 and below 1000 cm^{-1} corresponds to dabco skeletal motion. And

Table 1. Assignment of the major bands of the FT-IR spectra in the range of 4000 to 650 cm^{-1}.

Assignments	$KClO_4$	Raw-DAP-2	Nano-DAP-2	dabco	Assignments
C-H stretching		3182	3183	3235	C-H stretching
		3051	3051	2937	
				2870	CH_2 symmetric stretching vibration
				1678	CH_2 scissor
CH_2 scissor		1475	1476	1455	
		1422	1422	1314	C-N stretching
CH_2 wag or twist		1325	1325		
C-N stretching		1220	1220		
		1117	1118		
		1086	1086		
ClO_4^- stretching	1061	1064	1063	1056	dabco skeletal
Skeletal motion		1048	1047	991	CH_2 twist or wag
	939	889	890	904	dabco skeletal
		850	851	834	
		806	806	770	
				748	

for raw DAP-2, the peaks located at 3182, 3051 cm^{-1} correspond to C-H stretching and deformation vibrations. The spectrum peaks at 1475, 1422 cm^{-1} corresponds to CH$_2$ scissor of H$_2$dabco^{2+}. The peaks of the C-N stretching vibrations located at 1220, 1117, 1086 cm^{-1} and the ClO$_4^-$ at 1064 cm^{-1}. The IR peaks at 800–1048 cm^{-1} correspond to skeletal motion. The IR spectrum of raw DAP-2 shows C-H vibrational bands appeared red shift and the peak intensity change significantly compared with ClO$_4^-$ and babco due to the formation of C–H···O hydrogen bonds. However, the special case of the blue shift of C-H vibration bands are termed as anti-hydrogen bond type. As can be seen from Table 1, the IR peaks of the nano DAP-2 are similar to raw DAP-2, which indicates that the chemical structures of the material had not been changed during the ball-milling process.

The thermal decomposition performances of raw and nano DAP-2 were investigated at the heating rates of 5, 10, 15, 20°C·min^{-1} by DSC, as shown in Figure 3 and Table 2. The DSC curves have the same trend, such as two endothermic peaks (123 ~ 125°C and 308 ~ 311°C), and one exothermic peak from 365°C to 410°C at different heating rates. The onset temperatures of thermal decomposition increased with the heating rate increased. At the same heating rate, the thermal decomposition peaks of the nano DAP-2 sample have decreased due to the nano-effects (Guo et al. 2015), and the heat release become larger during the thermal decomposition process.

The Kissinger and Ozawa methods were used for calculating the kinetic parameters, the relationship between the decomposition peak temperatures and the heating rate can be described by the Kissinger Equation (1) and Ozawa Equation (2):

$$\ln\left(\frac{\beta}{T_p^2}\right) = \ln\frac{AR}{E_a} - \frac{E_a}{RT_p} \tag{1}$$

$$\lg\beta = \lg\left(\frac{AE_a}{Rg(\alpha)}\right) - 2.315 - 0.4567\frac{E_a}{RT} \tag{2}$$

Where β is the heating rate (°C·min^{-1}), T_p is the decomposition peak temperature, A is the pre-exponential factor, R is the ideal gas constant (8.314 J·mol^{-1}·K^{-1}), and E_a is the apparent activation energy.
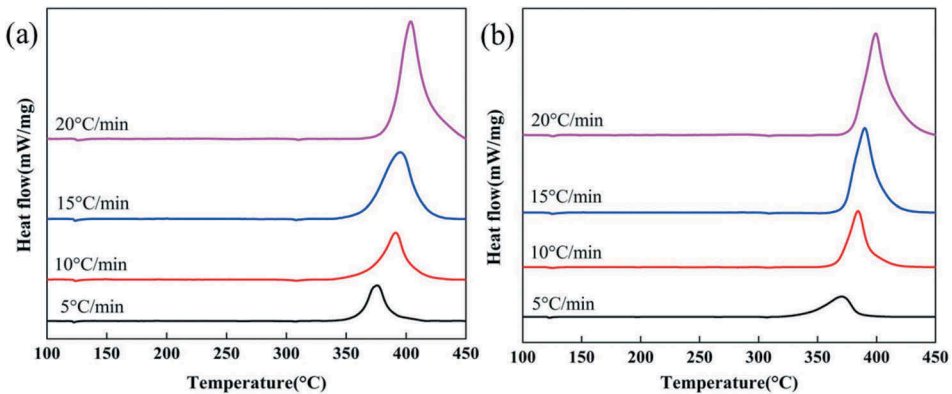

Figure 3. The DSC curves of (a) raw and (b) milling DAP-2 samples.

Table 2. Thermal data of DAP-2 samples at different heating rates.

Sample	T_p (°C)				E_a (kJ·mol^{-1})	
	5°C·min^{-1}	10°C·min^{-1}	15°C·min^{-1}	20°C·min^{-1}	kissinger	Ozawa
Raw DAP-2	375.7	391.2	395.3	403.8	177.699	175.311
nano DAP-2	370.2	384.5	390	399.7	170.297	165.438

Kissinger method is a differential processing method, which has the advantages of convenience and reliability. The kinetic parameters were calculated by the Kissinger method based on the conversion at the maximum thermal decomposition reaction point when the heating rate is different, and the characteristic temperature is selected to analyze the change of the reaction rate. Because the Kissinger method believed that the conversion rate α is independent of the reaction order, and assumed that the reaction rate at the peak temperature T_p of the thermal decomposition curve is the largest. The apparent activation energy E_a can be calculated according to the exothermic peak temperature T_p at different heating rates. And Ozawa method is an approximate integration method. The calculation of apparent activation energy E_a does not depend on the function form of $g(\alpha)$ and the choice of mechanism, so that the error caused by improper selection of mechanism function can be avoided. This method can be used as a verification method for the calculation of apparent activation energy.

The Kissinger plots of $\ln(\beta)$ versus $1000/T_p$, Ozawa plots of $\lg(\beta)$ versus $1000/T_p$ are shown in Figure 4. The apparent activation energy (E_a) of raw and nano DAP-2 is listed in Table 2. For raw DAP-2, the apparent activation energy is 177.699 kJ·mol^{-1} calculated by the Kissinger equation, and $E_a = 175.311$ kJ·mol^{-1} is verified by the Ozawa method. For nano DAP-2, the apparent activation energy is 170.297 kJ·mol^{-1} calculated by the Kissinger equation, and $E_a = 165.438$ kJ·mol^{-1} is verified by the Ozawa method. The apparent activation energy calculated by the two methods are in good agreement with each other, and the apparent activation energy of nano DAP-2 is lower than raw DAP-2, which indicated DAP-2 with nano sizes is easier to be active than raw materials due to nanostructure particles have a larger specific surface area, and more activated atoms and functional groups on the surfaces, which could be accelerated decomposition of substances.

Sensitivity performance is a key parameter to evaluate the safety of explosives, which indicates the degree of difficulty of explosion caused by external energy stimulate. In this work, the impact sensitivity was measured to characterize the safety performance of DAP-2 with different particle sizes. The impact sensitivity was expressed by the characteristic drop of 50% explosion probability caused by drop hammer (H_{50}). The special height (H_{50}) of raw DAP-2 is 36.79 cm, while the H_{50} of nano DAP-2 is 60.63 cm (The H_{50} data of some common explosives measured by the same experimental method are listed in Table 3). That indicated that the impact sensitivity of nano
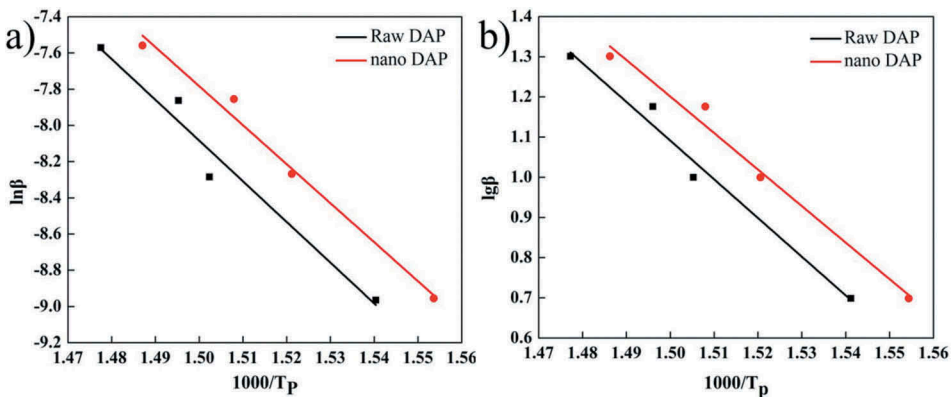

Figure 4. (a) The Kissinger plots of $\ln(\beta)$ versus $1000/T_p$ and (b) Ozawa plots of $\lg(\beta)$ versus $1000/T_p$.

Table 3. The H_{50} data of some common explosives.

Sample	Tetryl	TNT	RDX	HMX	Raw DAP-2	nano DAP-2
H_{50} (cm)	38	157	24	26	36.79	60.63

DAP-2 by the ball milling technology had been reduced. The nano DAP-2 exhibited more insensitivity properties, which can be explained by "hot spots" theory. On the one hand, nano-sized crystals are considered to have a more complete and uniform appearance. The micro crystal defects have been reduced by nano-sized treatments, resulting in a lower possibility of forming "hot spots" in the interior under external energy stimuli. On the other hand, the nearly spherical crystals formed by the ball milling method have good dispersion after being subjected to force, which makes the stress more uniformly dispersed and makes the possibility of the form "hot spots" lower. It is beneficial to reduce the impact sensitivity of the explosive by the nano-sized treatments. These results suggested that nano DAP-2 showed more safety property by the ball milling technology, which is of great significance to the practical application of DAP-2.

Conclusion

In summary, molecular perovskite $(H_2dabco)[K(ClO_4)_3]$ with nano size distributions from 1 μm to 2 μm were successfully prepared by mechanical ball milling technology. The crystal phase of DAP-2 explosive particles had no change during the ball milling process. The thermal exothermal peak temperature of nano DAP-2 are decreased by more than 6°C at the same heating rate. The apparent activation energy (Kissinger and Ozawa method: 170.297 kJ·mol^{-1} and 165.438 kJ·mol^{-1}) of nano DAP-2 had reduced than that of raw DAP-2 (177.699 kJ·mol^{-1}, 175.311 kJ·mol^{-1}), which demonstrated that the thermal decomposition of nano DAP-2 can be activated easier. The impact sensitivity of nano DAP-2 (H_{50}: 60.63 cm) is lower than that of raw DAP-2 (H_{50}: 36.79 cm). This work may provide a potential solution for the application of the advanced energetic materials with perovskite structure in practice application.

Conflicts of interest

There are no conflicts to declare.

References

Bennion, J. C., N. J. Chowdhury, J. W. Kampf, and A. J. Matzger. 2016. Hydrogen peroxide solvates of 2,4,6,8,10,12-Hexanitro-2,4,6,8,10,12-hexaazaisowurtzitane. *Angewandte Chemie International Edition* 55:1–5. doi:10.1002/ange.201607130.

Bolton, O., and A. J. Matzger. 2011. Improved stability and smart-material functionality realized in an energetic cocrystal. *Angewandte Chemie* 50:8960–63. doi:10.1002/anie.201104164.

Cao, X., L. Y. Yang, H. Y. Wang, Y. P. Shang, S. Q. Hu, P. Deng, and L. S. Hu. 2018b. Thermal decomposition and combustion characteristics of TKX-50 with network nanostructure fabricated by rapid freeze-drying method. *Chinese Journal of Energetic Materials* 26 (12):1044–48. doi:10.11943/CJEM2018294.

Cao, X., P. Deng, S. Q. Hu, L. J. Ren, X. X. Li, P. Xiao, and Y. Liu. 2018a. Fabrication and characterization of nanoenergetic hollow spherical hexanitrostibene (HNS) derivatives. *Nanomaterials* 8:336. doi:10.3390/nano8050336.

Cao, X., Y. Shang, K. Meng, Y. Liu, P. Deng, and L. Hu. 2019. Fabrication of three-dimensional TKX-50 network-like nanostructures by liquid nitrogen-assisted spray freeze-drying method. *Journal of Energetic Materials* 37:356–64. doi:10.1080/07370652.2019.1585491.

Chen, S. L., Y. Shang, C. T. He, L. Y. Sun, Z. M. Ye, W. X. Zhang, and X. M. Chen. 2018a. Optimizing the oxygen balance by changing the A-site cations in molecular perovskite high-energetic materials. *CrystEngComm* 20:7458–63. doi:10.1039/c8ce01350k.

Chen, S. L., Z. R. Yang, B. J. Wang, Y. Shang, L. Y. Sun, C. T. He, H. L. Zhou, W. X. Zhang, and X. M. Chen. 2018b. Molecular perovskite high-energetic materials. *Science China Materials* 61 (8):1123–28. doi:10.1007/s40843-017-9219-9.

Chen, W., L. Chang, S. B. Ren, Z. C. He, G. B. Huang, and X. H. Liu. 2020. Direct Z-scheme 1D/2D WO2.72/ZnIn2S4 hybrid photocatalysts with highly-efficient visible-light-driven photodegradation towards tetracycline hydrochloride removal. *Journal of Hazardous Materials* 384:121308. doi:10.1016/j.jhazmat.2019.121308.

Deng, P., H. Ren, and Q. J. Jiao. 2019a. Enhanced the combustion performances of ammonium perchlorate-based. *Vacuum* 169:108882. energetic molecular perovskite using functionalized graphene. doi:10.1016/j.vacuum.2019.108882.

Deng, P., H. Ren, and Q. J. Jiao. 2019b. Enhanced thermal decomposition performance of sodium perchlorate by molecular assembly strategy. *IONICS* Accepted. doi:10.1007/s11581-019-03301-0.

Deng, P., Y. Liu, P. Luo, J. X. Wang, Y. Liu, D. J. Wang, and Y. He. 2017. Two-steps synthesis of sandwich-like graphene oxide/LLM-105 nanoenergetic composites using functionalized graphene. *Materials Letters* 194:156–59. doi:10.1016/j.matlet.2017.02.038.

Deng, P., J. J. Xu, S. C. Li, S. L. Huang, H. B. Zhang, J. X. Wang, and Y. Liu. 2018. A facile one-pot synthesis of monodisperse hollow hexanitrostilbenepiperazine compound microspheres. *Materials Letters* 214:45–49. doi:10.1016/j.matlet.2017.11.104.

Deng, P., Q. J. Jiao, and H. Ren. 2020. Nano dihydroxylammonium 5,5'-bistetrazole-1,1'-diolate (TKX-50) sensitized by the liquid medium evaporation-induced agglomeration self-assembly, Accepted, doi:10.1080/07370652.2019.1695018.

Guo, X. D., G. Ouyang, L. Jie, L. Qing, L. X. Wang, Z. M. Gu, and F. S. Li. 2015. Massive preparation of reduced-sensitivity Nano CL-20 and its characterization. *Journal of Energetic Materials* 33 (1):24–33. doi:10.1080/07370652.2013.877102.

Hassanin, H., M. A. El-Sayed, A. ElShaer, K. Essa, and K. Jiang. 2018. Microfabrication of net shape Zirconia/Alumina nanocomposite micro parts. *Nanomaterials* 8 (8):593. doi:10.3390/nano8080593.

Hermann, T. S., K. Karaghiosoff, T. M. Klapötke, and J. Stierstorfer. 2017. Synthesis and Characterization of 2,2'-Dinitramino-5,5'-bi(1-oxa-3,4-diazole) and derivatives as economic and highly dense energetic materials. *Chemistry: A European Journal* 23 (50):12087–91. doi:10.1002/chem.201702191.

Lei, J., Q. Guo, D. Yin, X. D. Cui, R. He, T. Duan, and W. K. Zhu. 2019. Bioconcentration and bioassembly of N/S co-doped carbon with excellent stability for supercapacitors. *Applied Surface Science* 488:316. doi:10.1016/j.apsusc.2019.05.136.

Li, S. H., Y. Wang, C. Qi, X. X. Zhao, J. H. Zhang, S. W. Zhang, and S. P. Pang. 2013. 3D energetic metal-organic frameworks: Synthesis and properties of high energy materials. *Angewandte Chemie International Edition* 52:14031–35. doi:10.1002/ange.201307118.

Li, X. X., S. H. Hu, X. Cao, L. S. Hu, P. Deng, and Z. B. Xie. 2020. Ammonium perchlorate-based molecular perovskite energetic materials: preparation, characterization, and thermal catalysis performance with MoS2. *Journal of energetic materials. accepted.* doi:10.1080/07370652.2019.1679281.

Liu, W., L. W L, and S. P. Pang. 2017. Structures and properties of energetic cations in energetic salts. *RSC Advances* 7:3617–27. doi:10.1039/C6RA26032B.

Liu, Y., S. C. Li, J. J. Xu, H. L. Zhang, Y. X. Guan, H. Y. Jiang, S. L. Huang, H. Huang, and Z. S. Wang. 2018. Three Energetic 2,2',4,4',6,6'-Hexanitrostilbene cocrystals regularly constructed by H bonding, π stacking, and van der Waals interactions. *Crystal Growth & Design* 18 (4):1940–43. doi:10.1021/acs.cgd.8b00019.

Mo, Z., H. Xu, Z. G. Chen, X. J. She, Y. H. Song, J. B. Lian, X. W. Zhu, P. C. Yan, Y. H. Lei, S. Q. Yuan, and H. M. Li. 2019a. Construction of MnO2/Monolayer g-C3N4 with Mn vacancies for Z-scheme overall water splitting. *Applied Catalysis B: Environmental* 241:452–60. doi:10.1016/j.apcatb.2018.08.073.

Mo, Z., H. Xu, Z. G. Chen, X. J. She, Y. H. Song, J. B. Lian, X. W. Zhu, P. C. Yan, Y. H. Lei, S. Q. Yuan, and H. M. Li. 2019b. Constructing Pd/2D-C3N4 composites for efficient photocatalytic H2 evolution through nonplasmon-induced bound electrons. *Applied Surface Science* 467:151–57. doi:10.1016/j.apsusc.2018.10.115.

Qiu, H. W., R. B. Patel, R. S. Damavarapub, and V. Stepanov. 2015. Nanoscale 2CL-20·HMX high explosive cocrystal synthesized by bead milling. *CrystEngComm* 17:4080–83. doi:10.1039/c5ce00489f.

Tang, Y., L. A. Mitchell, G. H. Imler, D. A. Parrish, and J. M. Shreeve. 2017. Ammonia oxide as a building block for high-performance and insensitive energetic materials. *Angewandte Chemie International Edition* 56:5894–98. doi:10.1002/anie.201702285.

Tiruye, G. A., D. Muñoz-Torrero, T. Berthold, J. Palma, M. Antonietti, N. Fechlerb, and R. Marcilla. 2017. Functional porous carbon nanospheres from sustainable precursors for high performance supercapacitors. *Journal of Materials Chemistry* 5:16263–72. doi:10.1039/C7TA01951C.

Wang, J., Y. Q. Wang, Z. Q. Qiao, L. Zhang, P. Wu, and G. C. Yang. 2016. Self-assembly of TATB 3D architectures via microchannel crystallization and a formation mechanism. *CrystEngComm* 18. doi:10.1039/C5CE02436F.

Wang, L., S. Guan, Y. Weng, S. M. Xu, H. Lu, X. Meng, and S. Zhou. 2019. Highly efficient vacancy-driven photothermal therapy mediated by ultrathin MnO2 nanosheets. *Acs Applied Materials & Interfaces* 11:6267-6275. doi: 10.1021/acsami.8b20639.

Wang, Q. Y., S. Wang, X. Feng, L. Wu, G. Y. Zhang, M. R. Zhou, B. Wang, and L. Yang. 2017. A heat-resistant and energetic metal-organic framework assembled by chelating ligand. *ACS Applied Materials Interfaces* 9:37542–47. doi:10.1021/acsami.7b12767.

Wang, P. C., Y. G. Xu, Q. Wang, Y. L. Shao, Q. H. Lin, and M. Lu. 2019. Self-assembled energetic coordination polymers based on multidentate pentazole cyclo-N5-. *Science China Materials* 62 (1):122–29. doi:10.1007/s40843-018-9268-0.

Xu, J. J., S. S. Zheng, S. L. Huang, Y. Tian, Y. Liu, H. B. Zhang, and J. Sun. 2019. Host–Guest energetic materials constructed by incorporating oxidizing gas molecules into an organic lattice cavity toward achieving highly-energetic and low-sensitivity performance. *Chemical Communications* 55 (7):909–12. doi:10.1039/c8cc07347c.

Xu, Z., G. Cheng, H. Yang, X. Ju, P. Yin, J. Zhang, and J. M. Shreeve. 2017. A facile and versatile synthesis of energetic furazan-functionalized 5-Nitroimino-1,2,4-Triazoles. *Angewandte Chemie International Edition* 56 (21):5877–81. doi:10.1002/ange.201701659.

Zhang, S., Q. Yang, X. Y. Liu, X. N. Qu, Q. Wei, G. Xie, S. P. Chen, and S. L. Gao. 2016. High-energy metal–Organic frameworks (HE-MOFs): Synthesis, structure and energetic performance. *Coordination Chemistry Reviews* 307:292–312. doi:10.1016/j.ccr.2015.08.006.

Zhang, X., Z. C. Lai, Q. L. Ma, and H. Zhang. 2018. Novel structured transition metal dichalcogenide nanosheets. *Chemical Society Reviews* 47:3301–38. doi:10.1039/C8CS00094H.